

# Nondestructive measurement of machining-induced amorphous layers in single-crystal silicon by laser micro-Raman spectroscopy

Jiwang Yan\*, Tooru Asami, Tsunemoto Kuriyagawa

*Department of Nanomechanics, School of Engineering, Tohoku University, Aramaki Aoba 6-6-01, Aoba-ku, Sendai 980-8579, Japan*

Received 2 April 2007; received in revised form 19 July 2007; accepted 13 August 2007  
Available online 13 October 2007

## Abstract

Laser micro-Raman spectroscopy was used to examine silicon wafers precision machined by diamond tools, and the results were compared with transmission electronic microscopic results. It was found that near-surface amorphous layers were generated by machining and there was a strong correlation between the thickness of the amorphous layer and the Raman intensity ratio of the amorphous phase to the crystalline phase. This finding provides the feasibility of a fast, inexpensive, nondestructive and quantitative measurement approach for subsurface damages of semiconductor materials by using laser micro-Raman spectroscopy. The effective measurement range was experimentally investigated and the sensing limits were theoretically discussed from the aspect of light scattering and light absorption with a double-layer material model.

© 2007 Elsevier Inc. All rights reserved.

**Keywords:** Silicon; Ultraprecision machining; Ductile machining; Laser micro-Raman; Phase transformation; Subsurface damage; Amorphous; Nondestructive evaluation

## 1. Introduction

Single-crystal silicon is not only a dominant substrate material for the fabrication of microelectronic and micromechanical components but also an important infrared optical material [1,2]. Although silicon is a nominally brittle material, it can be deformed in a ductile manner in precision machining processes, yielding continuous ductile chips and smooth surfaces [3–8]. However, machining will inevitably cause subsurface damages such as phase transformations, dislocations and potential microcracks. It is the depth and nature of the subsurface damages that influences the mechanical, optical and electronic performances of silicon products [9]. Usually, subsequent chemical etching and/or chemo-mechanical polishing (CMP) processes are necessary to remove the subsurface damage layers for defect-free silicon substrates. A recent work of the present authors has also demonstrated that nanosecond-pulsed laser irradiations can be used to reconstruct the machining-damaged silicon substrates to perfect single crystalline structures, which provides the pos-

sibility of a new processing technique for high quality silicon wafers [10].

In order to determine optimal processing conditions for the CMP and laser irradiation, quantitative measurement of the subsurface damage depth is an essential step. Quick, nondestructive and low-cost measurement of subsurface damage depth has become a subject of concentrated research interests in the semiconductor manufacturing industry. Small-tool polishing and slanted polishing methods can be used to measure the depth of microcracks induced by machining [11]. However, these techniques are not sufficiently sensitive for measuring the depths of the phase transformation layers which are usually ranging from ten-nanometer level to the submicron level.

A number of previous authors used cross-sectional transmission electron microscopes (TEM) to observe the subsurface microstructures of machined silicon wafers. TEM studies of diamond-turned silicon surfaces conducted by Shibata et al. revealed that a 150-nm-thick amorphous layer was formed by machining, below which is a region of crystal about 2–3  $\mu\text{m}$  deep deformed by shear dislocation loops [12]. The TEM results of Jeynes et al. showed that a 110-nm-thick amorphous layer, below which a dislocated crystalline region about 260 nm deep, was formed during diamond turning [13]. Puttick et al.

\* Corresponding author. Tel.: +81 22 795 6946; fax: +81 22 795 7027.  
E-mail address: [yanjw@pm.mech.tohoku.ac.jp](mailto:yanjw@pm.mech.tohoku.ac.jp) (J. Yan).

demonstrated that the total depth of the subsurface damages, including amorphous layers and dislocations, of both diamond turned and ground silicon is in the range of 100–400 nm [14].

TEM enables precise measurement of subsurface damages. However, to make a TEM specimen, the workpiece needs to be processed to extremely thin, namely in 10–100 nm level, by ion milling or focused ion beam (FIB) techniques. From this point of view, TEM method is a destructive evaluation method, also expensive and time consuming. On the other hand, recently, the needs for rapid and nondestructive measurement of subsurface damage depth at a low-cost keep increasing. This is due to the fact that the depth of subsurface damages changes significantly with machining conditions such as depths of cut, tool geometries and crystal orientations of workpiece, and it is still difficult to precisely predict the relationship between the subsurface damage depth and the machining conditions.

In the present work, we attempted to measure the depth of the phase transformation layer resulting from diamond machining by using laser micro-Raman spectroscopy. We proposed a new parameter based on Raman spectra, namely Raman intensity ratio, and investigated the relationship between this ratio and the TEM results. It is expected that this parameter can be used for quantitative measurement of subsurface damage depth of silicon. This measurement method, if successful, will be very quick, inexpensive and completely nondestructive. Other advantages of laser Raman measurement include that it can be done at room temperature, in air and without contacts. It can also be used for on-machine measurement and mapping of specific surface areas. Furthermore, the measurement of subsurface damages can be combined with residual stress measurement by using a single Raman system.

## 2. Laser Raman spectra analysis

Laser micro-Raman spectroscopy has been known as a powerful characterization technique for various semiconductor and insulator materials. The Raman effect is based on the inelastic scattering of laser [15]. Fig. 1 schematically shows the principle of laser scattering. Scattering occurs when a beam of monochromatic light passes through a crystal, and the scattering involves

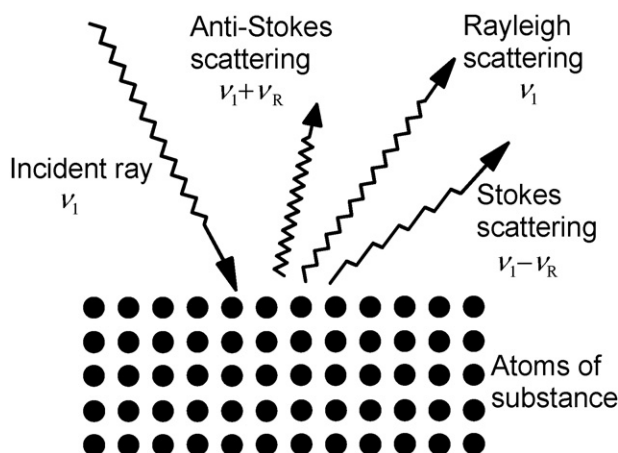


Fig. 1. Schematic model of laser scattering.

Rayleigh scattering and Raman scattering. The Rayleigh scattering is caused by the elastic collision between the incident photons with the phonons in materials, thus generates light with the same vibration frequency as the incident ray. On the other hand, the Raman scattering is induced by the inelastic collision between the incident photons with the phonons in materials, hence produces light with different vibration frequency. In the Raman scattering, the scattered light with vibration frequency  $\nu_1 - \nu_R$  is called Stokes, and those  $\nu_1 + \nu_R$  is called anti-Stokes, where  $\nu_R$  ( $\nu_R > 0$ ) is the Raman shift. The Raman shift is strongly influenced by microscopic structural changes, impurity and residual strains, which lead to changes in phonon frequencies, broadening of Raman peaks, and breakdown of Raman selection rules.

Laser Raman can detect the presence of amorphous silicon as well as residual stresses in silicon wafers. For bulk crystalline silicon (c-Si), the triple degenerate optical phonons display in the first-order Raman spectrum a sharp peak at the Raman shift of  $521 \text{ cm}^{-1}$ , and for amorphous silicon (a-Si), the first-order Raman spectrum reflects the phonon density of states and presents an optical band peak at  $470 \text{ cm}^{-1}$  [16–18]. Raman scattering has been used to detect the structural change and residual stress of silicon in scratching, dicing, lapping, grinding and diamond turning processes [19–24]. Chen et al. also attempted to measure the depth of subsurface damage by incorporating laser Raman with repetitive chemical etching processes [25]. However, to date, no literature can be found on completely nondestructive and quantitative measurements of the subsurface damage depth by using laser Raman only.

In most of previous works, qualitative detection of structural changes of materials has been carried out using Raman shift information, whereas the intensity information of the Raman scattering has not been effectively used. In the present work, we attempt to use the Raman intensity to characterize the thin amorphous layers on the crystalline bulk material. In order to compare the intensities of Raman scattering from the amorphous region and that from the crystalline region, we propose a new parameter, namely Raman intensity ratio  $r$ , to represent the relative significance of the two phases. Raman intensity ratio  $r$  is defined by

$$r = \frac{I_a}{I_c} \quad (1)$$

where  $I_a$  is the total Raman intensity of the amorphous silicon, and  $I_c$  is the total Raman intensity of the crystalline silicon. It can be seen that the bigger the value of  $r$ , the thicker the amorphous layer. In the equation, the total Raman intensities,  $I_a$  and  $I_c$ , are defined as the integrations of the amorphous and crystalline Raman peaks with respect to the Raman shift. Compared to the maximum peak value, the total Raman intensity can precisely represent the laser scattering at different vibration frequencies.

On many occasions, the Raman spectra of a machined surface contain two neighboring peaks: a sharp crystalline peak at  $521 \text{ cm}^{-1}$  and a broadband amorphous peak around  $470 \text{ cm}^{-1}$  [21–24], and the two peaks overlap each other, as schematically shown in Fig. 2(a). For this reason, it is difficult to directly obtain the integrations of Raman intensities of individual peaks from

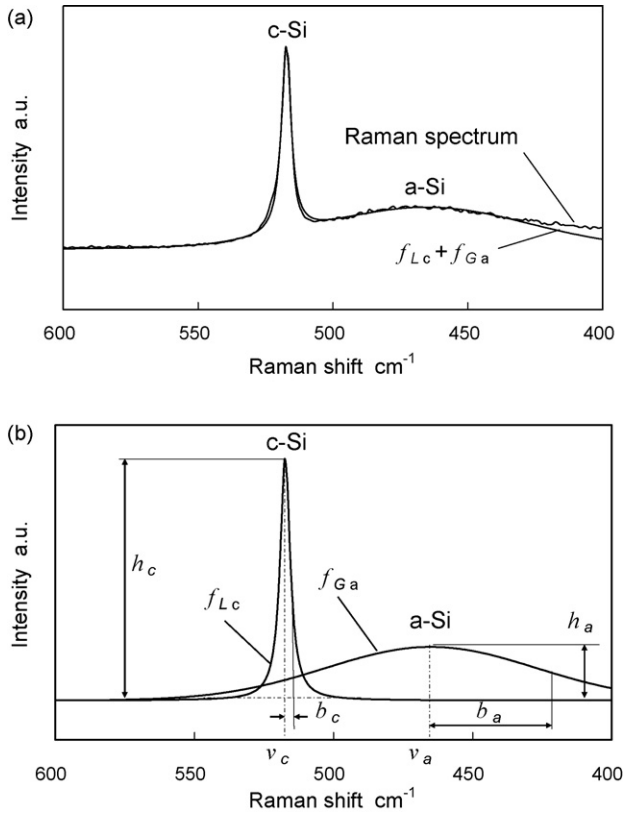


Fig. 2. Curve fitting method for separating Raman peaks: (a) comparison of experimental Raman spectra and fitted curve; (b) separated Raman peaks of amorphous and crystalline silicon.

the raw Raman spectra. Raman peak separation from the spectra is necessary.

Curve fitting is an effective technique for separating overlapping peaks. Gaussian distribution and Lorentzian distribution are two common functions used for fitting light spectra in optical area. Generally speaking, the Gaussian distribution, also known as the normal distribution, is suitable for fitting broadband curves in continuous probability problems; whereas the Lorentzian distribution is suitable for describing the line shape of spectral lines which are broadened by various mechanisms such as collision, or other sharp peaks in spectroscopy. In the present work, for the fact that the amorphous peaks in the Raman spectra are broadband ones while the crystalline peaks are sharp ones, we used the Gaussian distribution for fitting amorphous peaks and the Lorentzian distribution for fitting crystalline peaks, respectively. In this way, higher fitting accuracy can be achieved compared to using either single fitting function.

The functions of Gaussian distributions  $f_{Ga}$  and Lorentzian distribution  $f_{Lc}$  with respect to Raman shift  $\nu$  can be shown as follows:

$$f_{Ga}(\nu) = h_a \exp \left\{ -\frac{(\nu - \nu_a)^2}{b_a^2} \right\} \quad (2)$$

$$f_{Lc}(\nu) = \frac{h_c}{1 + (\nu - \nu_c)^2/b_c^2} \quad (3)$$

where  $\nu_a$  and  $\nu_c$  are the Raman shifts,  $h_a$  and  $h_c$  are the heights,  $b_a$  and  $b_c$  are the half-power bandwidths of the amorphous and crystalline peaks, respectively. Therefore, the Raman intensity ratio  $r$  in Eq. (1) can be obtained by

$$r = \frac{\int f_{Ga}(\nu) d\nu}{\int f_{Lc}(\nu) d\nu} = \frac{h_a b_a \sqrt{\pi}}{h_c b_c \pi} = \frac{1}{\sqrt{\pi}} \frac{h_a b_a}{h_c b_c} \quad (4)$$

To automatically perform curve fitting of the Raman peaks, a computer program based on the least squares method was developed in the present work. Using the program, the synthetic curve  $f_{Ga} + f_{Lc}$ , namely the sum of the amorphous peak and the crystalline peak, can be fitted to coincide with the experimental Raman spectra in a few tens of seconds. It should be pointed out that the baseline of Raman spectra, where the theoretical Raman intensity is zero, sometimes goes up and down due to the background noise or drift of the Raman system. To avoid the drifts and noises, at first we offset the baseline of the Raman spectra to zero before curve fitting.

An example of curve fitting result is given in Fig. 2(a). It can be seen that the fitted curve  $f_{Ga} + f_{Lc}$  is generally consistent with the experimental Raman spectra and the fitting error is ignorable. Then the curves  $f_{Ga}$  and  $f_{Lc}$  are separated and the parameters  $h_a$ ,  $h_c$ ,  $b_a$  and  $b_c$  can be simply readout from the individual curves of  $f_{Ga}$  and  $f_{Lc}$ , as shown in Fig. 2(b). Finally, the Raman intensity ratio  $r$  can be calculated immediately according to Eq. (4). Next, the relationship between the Raman intensity ratio and the thickness of the amorphous layer will be examined experimentally.

### 3. Experimental procedures

#### 3.1. Machining tests

In the present experiments, plunge-cutting method is used for obtaining a continuous change in depth of cut during one single cut. The cutting tool is subjected to a transverse feed in the horizontal direction while the depth of cut changes continuously in the vertical direction. In this way, microgrooves with varying depth can be produced. The longitudinal cross-section of the microgroove is schematically shown in Fig. 3. Machining tests were done with an ultraprecision lathe Toyoda AHN-05, which enables tables to move under four-axis (XYZB) numerical control at a stepping resolution of 1 nm. The cutting tool is made of single-crystal diamond and has a nose radius of 10 mm. The tool rake angle was changed from  $0^\circ$  to  $-60^\circ$ , and depth of

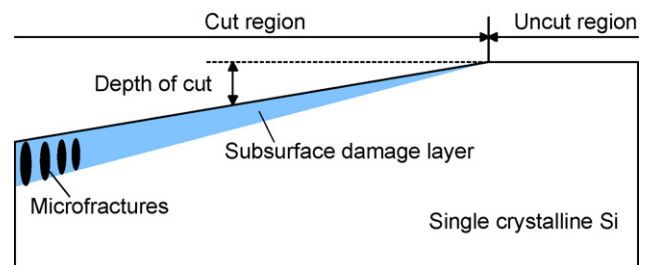


Fig. 3. Schematic model of a plunge-cut microgroove.

cut was changed from 0 to 500 nm. The cutting speed was fixed to 500 mm/min. As workpiece, an electric device grade n-type single-crystal silicon (1 0 0) wafer was machined. The wafer is 150 mm in diameter, 550  $\mu\text{m}$  in thickness and obtained with a chemomechanical polished finish. As lubricant and coolant, the Bluebe #LB10 cutting oil was used in the form of mist jet.

### 3.2. Laser micro-Raman tests

The machined silicon samples were examined using a laser micro-Raman spectroscope, NRS-3100, produced by JASCO Corporation (Tokyo, Japan). The wavelength of the laser was 532 nm and the output laser power was set to 10 mW. A 100 $\times$  objective lens with a numerical aperture (NA) of 0.95 was used so that the focused laser spot size was 1  $\mu\text{m}$ . This spot size was easily to be pointed to any locations within the machined groove to investigate the subsurface damages at different depths of cut. In order to diminish experimental errors, all of the measurements were performed under the same strictly controlled conditions at room temperature.

### 3.3. TEM observations

In order to confirm the depth of the subsurface damages and compare with the laser micro-Raman results, cross-sectional observations of the specimen were performed with a TEM. The TEM samples were cut out from the silicon wafer and thinned to about 100 nm by the FIB technique to enable electron transmission. The TEM we used was H-9000NAR, produced by Hitachi Ltd. (Tokyo, Japan). The acceleration voltage used for TEM observations were 300 kV. To protect from possible damages from the FIB, carbon (C) and tungsten (W) coatings were made on the samples.

## 4. Results and discussion

### 4.1. Typical Raman spectra

Two typical examples of Raman spectra will be shown here. Fig. 4(a) is the Raman spectrum of a surface machined at a depth of cut of 60 nm. There are two characteristic peaks in the spectrum: a sharp peak at 521  $\text{cm}^{-1}$  and a broadband peak centered at 470  $\text{cm}^{-1}$ . This is the typical Raman spectrum for a diamond-machined silicon surface, which demonstrates that the near-surface layer has been transformed into the amorphous state. However, the crystalline peak is still significant in the spectrum, indicating that the amorphous layer is relatively thin so that the Raman response from the bulk crystalline region could be strongly detected from the surface.

Fig. 4(b) is the Raman spectrum of a surface machined at a depth of cut of 120 nm. The broadband peak at 470  $\text{cm}^{-1}$  has grown significantly compared to that in Fig. 4(a), whereas the peak at 521  $\text{cm}^{-1}$  becomes extremely small. The lack of feature at 521  $\text{cm}^{-1}$  is indicative of the increase in the thickness of amorphous layer. That is, the Raman-scattered light from the deep bulk crystalline region becomes very weak.

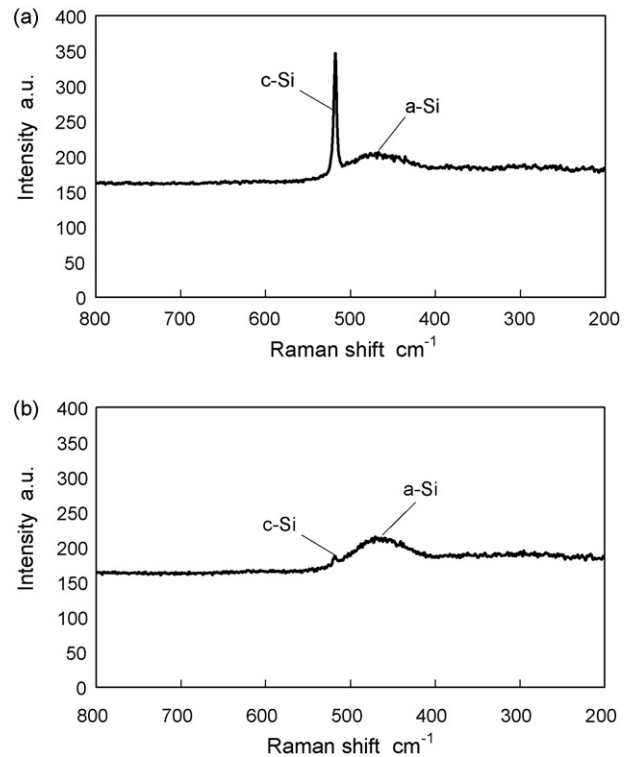


Fig. 4. Laser micro-Raman spectra of surface regions machined at various depths of cut: (a) 60 nm and (b) 120 nm.

### 4.2. TEM observation results

Cross-sectional TEM observations were done for five samples. Fig. 5(a) is a TEM micrograph of the sample machined under the same conditions as that shown in Fig. 4(a). An averagely 63-nm-thick grey layer can be seen under the cut surface. It is empirically assumed that this grey layer should be the machining-induced phase transformation layer. Below the phase transformation layer, there is a thin dislocated layer with a few dislocations extending into the deep region.

Fig. 5(b) is a TEM micrograph of the sample machined under the same conditions as that shown in Fig. 4(b). In this case, the grey layer is approximately 125-nm-thick, significantly thicker than that in Fig. 5(a). Below the grey layer, intensive dislocations can be seen in the crystalline region.

To confirm the microstructure of the grey layers, selected area diffraction analysis was made using the same TEM. Fig. 6 shows the diffraction pattern of the grey layer shown in Fig. 5(b). In the figure, only halo rings are shown, verifying that the grey layer just beneath the machined surface is amorphous.

### 4.3. Comparison of Raman and TEM results

Raman intensity ratios were calculated according to the method mentioned in Section 2, and plotted in Fig. 7 against the thickness of amorphous layers measured by TEM. Because the Raman intensity ratio undergoes drastic changes to the change of amorphous layer depth, the logarithmic coordinate was used for the vertical axis of the graph. In the figure, an error bar is

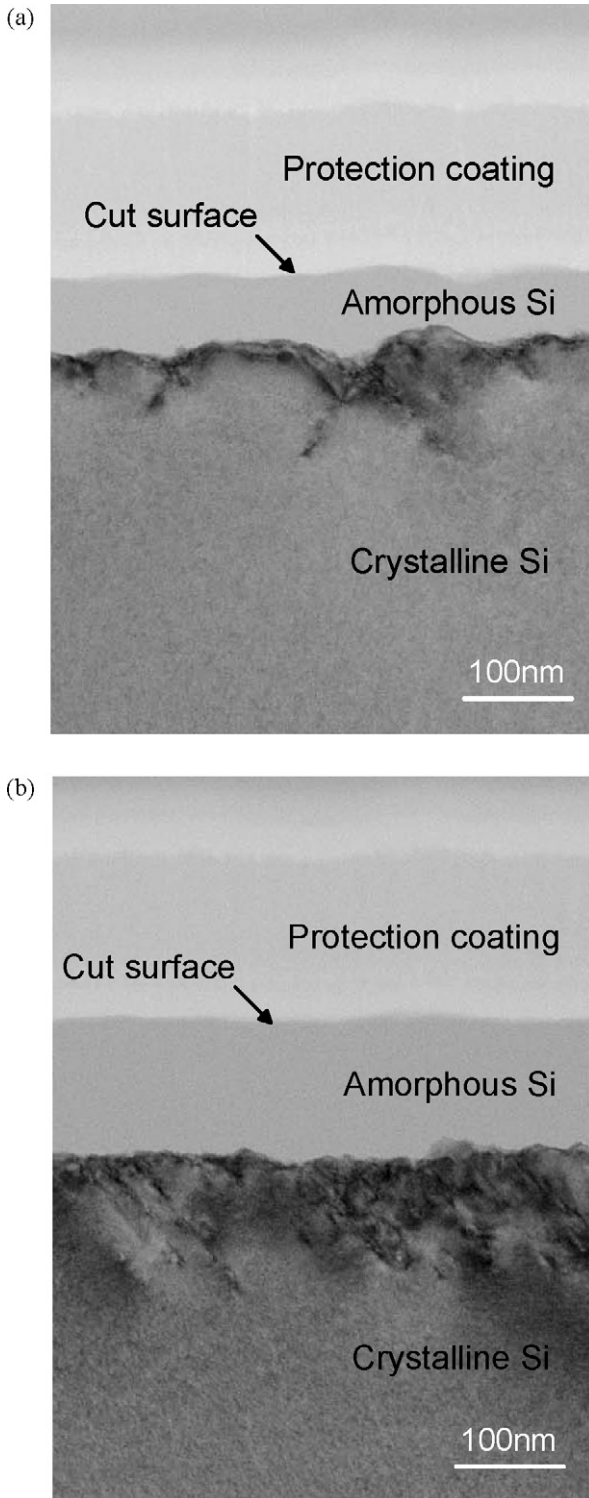


Fig. 5. Cross-sectional TEM micrographs of the samples machined at various depths of cut: (a) 60 nm and (b) 120 nm.

given to the leftmost data point, showing the variation range of the Raman intensity ratio during five Raman measurements at the same point. Error bars of other data points were not given because they were too short to be clearly shown in the figure. Although the number of data points is limited, a clear correlation can be identified between the Raman intensity ratio and the

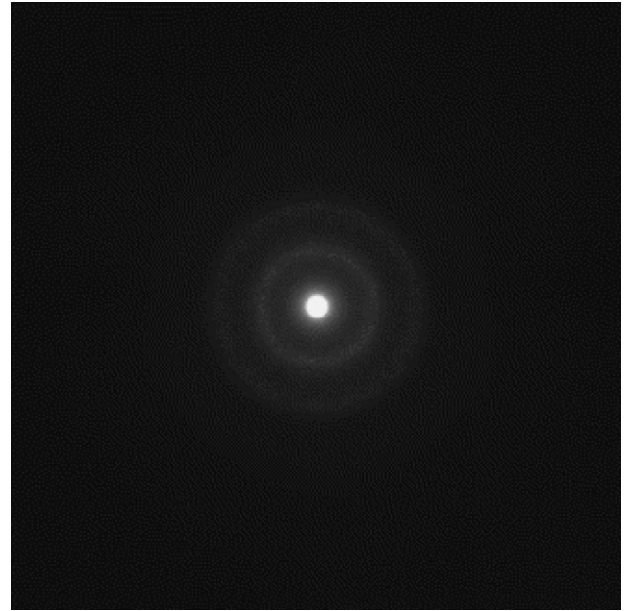


Fig. 6. Selected area diffraction pattern of the grey layer in Fig. 5(b). The halo rings indicate a complete amorphous structure.

depth of amorphous layer. It is noteworthy that the correlation is approximately linear within the experimental range. Therefore, by utilizing the linear relationship, it is possible for us to quantitatively measure the depth of amorphous layers using the Raman intensity ratio.

#### 4.4. On the effective measurement range

It must be pointed out that the Raman intensity ratio is meaningful only when both the crystalline peak and the amorphous peak simultaneously appear in the Raman spectra. If the amorphous layer is too thin to generate detectable Raman scattering around  $470\text{ cm}^{-1}$ , or the amorphous layer is too thick to let the Raman-scattered light from the bulk crystalline region ( $521\text{ cm}^{-1}$ ) to be detected from the surface, there will be only one visible peak in the Raman spectra. On those occasions, the Raman intensity ratio cannot be calculated. In other words, there are an upper sensing limit and a lower sensing limit in the depth range of the amorphous layer.

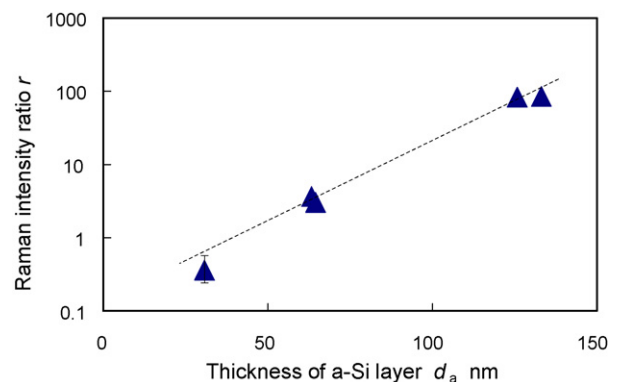


Fig. 7. Plot of Raman intensity ratio versus amorphous layer thickness.

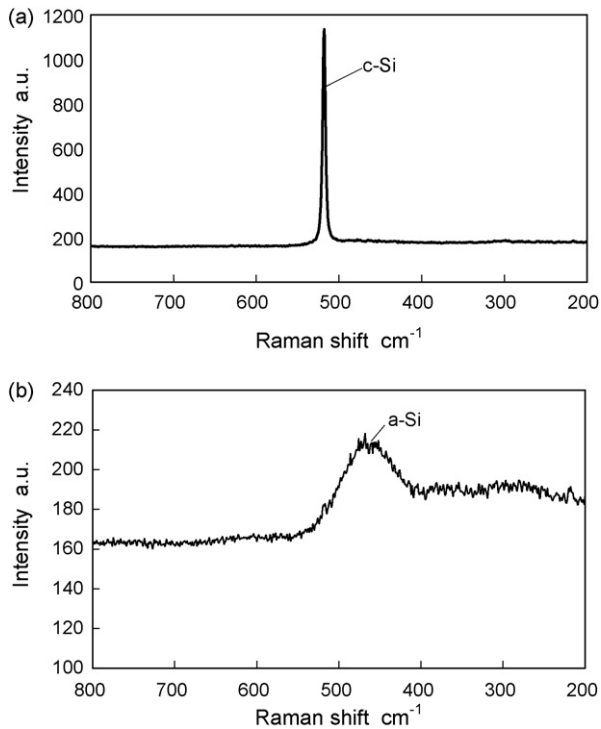


Fig. 8. Raman spectra showing only crystalline peak (a) and only amorphous peak (b).

For example, Fig. 8(a) shows Raman spectra of a machined silicon surface at a depth of 5 nm. No obvious amorphous peak at 470 cm<sup>-1</sup> can be found in the Raman spectra and there is only a sharp peak at 521 cm<sup>-1</sup>. This result indicates that the machining-induced amorphous layer is too thin to cause detectable Raman scattering. Fig. 8(b) shows the Raman spectra of the surface machined at a depth of 150 nm. In this case, although a very significant broadband peak is shown around 470 cm<sup>-1</sup>, no peak can be identified at 521 cm<sup>-1</sup>, which indicates that the amorphous layer is excessively thick.

To find the sensing limits of amorphous layer depth, Raman test points were moved along the plunge-cut microgroove. Assuming that the thickness of the amorphous layer is proportional to the depth of cut in plunge cutting, we found that the upper and lower sensing limits were around 10 and 150 nm, respectively.

It is also considered that near the sensing limits, the correlation between the Raman intensity ratio and the amorphous layer thickness shown in Fig. 7 will become nonlinear. Due to the high cost of TEM sample preparation, it is not realistic to experimentally identify the exact trend of the curve around the sensing limits by TEM observation. Alternatively, we carried out an analytical prediction on this issue in the appendix of this paper by modeling the laser absorption and laser scattering with an amorphous/crystalline double-layer material model. From the analysis in the appendix, we found that the theoretical relationship between the Raman intensity ratio and the amorphous layer thickness is approximately linear in the range from 20 to 140 nm; whereas beyond this range, nonlinearity occurs. Fortunately, the range of 20–140 nm covers most of

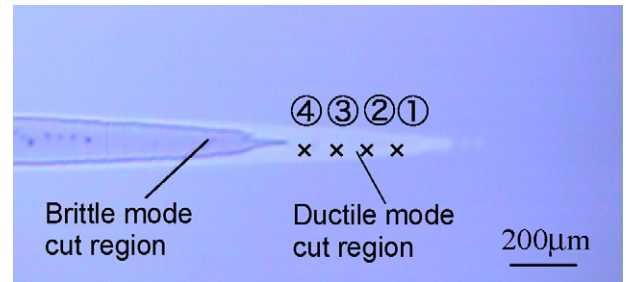


Fig. 9. Micrograph of the plunge-cut microgroove for Raman tests at high laser intensity levels.

the machining-induced amorphous layer depths reported in the literature [10,12–14,26,27]. Therefore, a linear approximation is applicable to silicon surfaces produced by various precision machining processes, including single-point machining and abrasive machining. It should be pointed out that for abrasive-machined surfaces, Raman spectra may change significantly with test point locations. One of the reasons for this phenomenon might be the nonuniformity of subsurface microstructure resulting from multipoint abrasive grains with irregular shapes.

#### 4.5. On the laser intensity level

As known from the appendix, theoretically the sensing limits of laser Raman can be extended by using a higher laser intensity level. In order to verify this effect, Raman tests were done at an elevated laser intensity level of 30 mW, three times that of the usual level (10 mW), while other conditions were kept the same. Fig. 9 is a micrograph of the plunge-cut microgroove where the Raman test points are marked by numbers 1–4. The depths of cut for points 1–4 are 30, 45, 60 and 75 nm, respectively, within the ductile machining regime.

Fig. 10(a) shows the Raman spectra of the four test points at the usual laser intensity level (10 mW). It can be seen that from point 1 to 4, the height of crystalline peak becomes lower and lower while the amorphous band becomes more and more obvious, indicating a growing amorphous layer with depth of cut. Fig. 10(b) is the Raman spectra of the same test points at the elevated laser intensity level (30 mW). Compared to Fig. 10(a), the intensities of both the crystalline peaks and the amorphous peaks have become stronger for all the points. This fact demonstrates that by using higher laser intensity levels, the sensitivity of Raman system can be significantly improved. However, it is also noticed that in Fig. 10(b), the results of points 3 and 4 involve new peaks at 510 cm<sup>-1</sup>. As known from previous studies, these new peaks correspond to micro-crystalline silicon (polycrystalline silicon, p-Si) [28]. Therefore, it can be said that at this laser intensity level, recrystallization of amorphous silicon has occurred, which is similar to the phenomena in laser crystallization processes [29,30]. In this case, precise measurement of the amorphous layer depth will be difficult.

Several other techniques may be used to extend the effective measurement range of the proposed method. One is to use longer exposure time and higher resolution detectors. Another way is to use multi-wavelength lasers as excitation source for the Raman

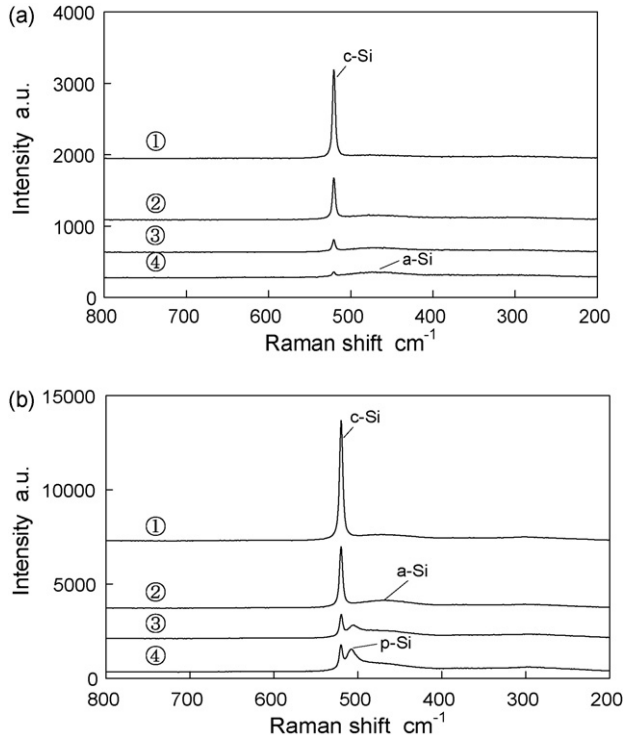


Fig. 10. Raman spectra of the four test points marked in Fig. 9, obtained at different laser intensity levels: (a) 10 mW and (b) 30 mW.

system, which enables variable penetration depths of lasers into the silicon wafer. These issues will be further investigated in the future.

## 5. Conclusions

Laser micro-Raman spectroscopy has been used to examine silicon wafers plunge-cut by diamond tools, and the Raman results were compared to the TEM results. The following conclusions have been obtained:

- (1) A new parameter called Raman intensity ratio was proposed to represent the significance of machining-induced amorphization of silicon. The ratio can be simply obtained from the Gaussian- and Lorentzian-fitted curves of the Raman peaks.
- (2) A strong correlation can be identified between the logarithm of Raman intensity ratio and the thickness of amorphous layer, and the correlation is approximately linear within the experimental range.
- (3) The upper and the lower sensing limits are approximately 10 and 150 nm, respectively. Near the sensing limits, nonlinearity occurs to the correlation between the Raman intensity ratio and the amorphous layer thickness.
- (4) At an elevated laser intensity level, the sensitivity of the Raman system can be significantly improved, but amorphous silicon undergoes micro-crystallization.

The present work has demonstrated the feasibility of fast, nondestructive, inexpensive and quantitative measurement of

machining-induced subsurface damages of silicon by using laser Raman spectroscopy. Upon calibration, this method should also be applicable to other materials. Future work includes performing on-machine mapping measurement by using the proposed measurement method to assist the investigation of subsurface damaging mechanism and the improvement of subsurface integrity of semiconductor substrates and optical components.

## Acknowledgements

Thanks are extended to the JASCO Corporation for the assistance with high intensity level laser micro-Raman tests. J. Y. also would like to acknowledge the financial supports from the Japan New Energy and Industrial Technology Development Organization (NEDO).

## Appendix A

### A.1. Laser intensity loss in Raman scattering

In order to understand the correlation between the Raman intensity ratio and the amorphous layer thickness, theoretical analysis will be carried out in this section by considering the laser intensity loss due to absorption and scattering. First, we discuss the laser response using a single-layer material model as shown in Fig. A1. Consider a small volume element in the material the thickness of which is  $dz$  and the distance from which to the surface is  $z$ . If we suppose that the initial intensity of the incident laser is  $I_0$ , and when reaching the volume element the intensity becomes  $I_z$ , and that the absorption coefficient and the scattering coefficient are  $\kappa$  and  $\sigma_s$ , respectively, then the laser intensity loss  $dI_z$  caused by the volume element can be written as

$$dI_z = -\kappa I_z dz - \sigma_s I_z dz = -(\kappa + \sigma_s) I_z dz \quad (A1)$$

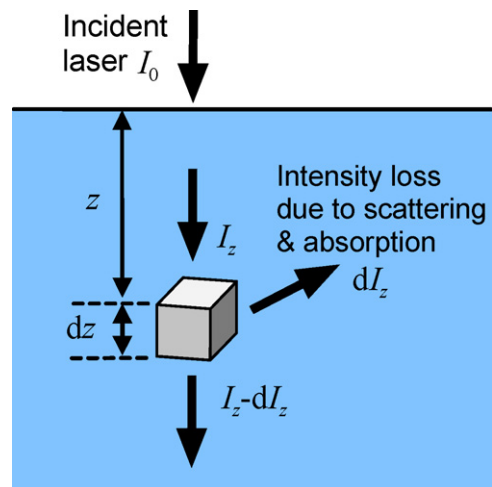


Fig. A1. Schematic model of laser intensity loss due to scattering and absorption in a single-layer material.

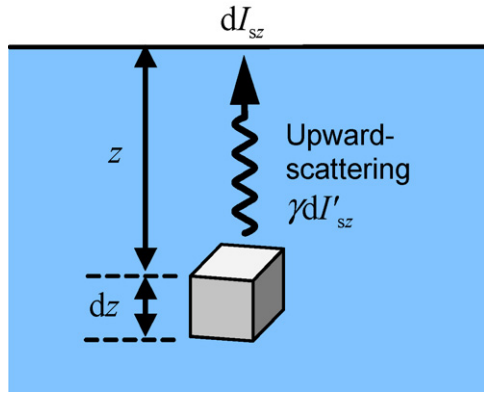


Fig. A2. Schematic model of upward-scattered laser intensity.

The boundary condition at the surface ( $z=0$ ) is  $I_z=I_0$ . Thus, after integration we obtain

$$I_z = I_0 \exp\{-(\kappa + \sigma_s)z\} \quad (\text{A2})$$

For simplicity, we define a total intensity loss coefficient (attenuation coefficient)  $\alpha$  as

$$\alpha = \kappa + \sigma_s \quad (\text{A3})$$

Then Eq. (A2) becomes

$$I_z = I_0 \exp(-\alpha z) \quad (\text{A4})$$

Next, we consider laser scattering from the volume element. The intensity of the scattered light from the volume element  $dI'_{sz}$  can be written as

$$dI'_{sz} = \sigma_s I_z dz = \sigma_s I_0 \exp(-\alpha z) dz \quad (\text{A5})$$

As shown in Fig. A2, while the laser scatters towards all directions, only the upward scattered light  $\gamma dI'_{sz}$  can be finally detected from the surface, where  $\gamma$  is the ratio of the upward scattered light to the totally scattered light. The upward scattered light is further attenuated due to absorption and scattering, thus the final output light at the surface  $dI_{sz}$  becomes

$$dI_{sz} = \gamma dI'_{sz} \exp(-\alpha z) = \gamma \sigma_s I_0 \exp(-2\alpha z) dz \quad (\text{A6})$$

Therefore, using the boundary condition  $I_{sz}=0$  at the surface, we can obtain the totally upward scattered light from the subsurface region as

$$I_{sz} = \frac{\gamma \sigma_s}{2\alpha} I_0 \{1 - \exp(-2\alpha z)\} \quad (\text{A7})$$

### A.2. Maximum sensing depth

Next, we use a double-layer material model to represent the subsurface structure of machining-damaged silicon wafers. As shown in Fig. A3, crystalline silicon is covered by an amorphous silicon layer of depth  $d_a$ . Here we suppose the minimum light intensity which can be detected from the surface by the Raman system is  $I_{\min}$  which corresponds to a sensing depth  $D$  ( $D > d_a$ ). If the exposure time and sensitivity of the detector are fixed,  $I_{\min}$  will be a constant.

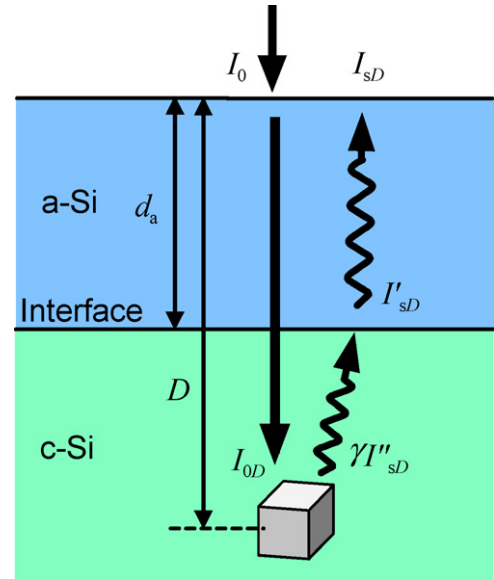


Fig. A3. Laser scattering model for a double-layer material structure, showing the maximum sensing depth.

Consider a small volume element located at a depth  $D$ . When the incident laser  $I_0$  reaches the volume element, the intensity  $I_{0D}$  will be

$$I_{0D} = I_0 \exp\{-\alpha_a d_a - \alpha_c (D - d_a)\} \quad (\text{A8})$$

where  $\alpha_a$  and  $\alpha_c$  are the total intensity loss coefficients of a-Si and c-Si, respectively. Then the upward-scattered light from this element will be attenuated again by the crystalline region and the amorphous layer before reaching the surface. Thus,  $I_{\min}$  can be expressed as

$$\begin{aligned} I_{\min} &= I'_{\min} \exp(-\alpha_a d_a) = \gamma I''_{\min} \exp\{-\alpha_c (D - d_a)\} \exp(-\alpha_a d_a) \\ &= \gamma \sigma_{sc} I_{0D} \exp\{-\alpha_c (D - d_a) - \alpha_a d_a\} \\ &= \gamma \sigma_{sc} I_0 \exp\{-2\alpha_c (D - d_a) - 2\alpha_a d_a\} \end{aligned} \quad (\text{A9})$$

where  $\sigma_{sc}$  is the scattering coefficient of c-Si. For simplicity, we let

$$\beta = \gamma \sigma_{sc} \exp\{-2\alpha_c (D - d_a) - 2\alpha_a d_a\} \quad (\text{A10})$$

Then Eq. (A9) can be changed into

$$I_{\min} = \beta I_0 \quad (\text{A11})$$

To find the relationship between  $D$  and  $d_a$  using Eq. (A10), we consider a boundary condition  $D = d_a$ , which means that the amorphous layer has just the thickness to isolate the scattered light from the crystalline region. In this case, only the amorphous peak will be seen in the Raman spectra. Thus  $\beta$  becomes

$$\beta = \gamma \sigma_{sc} \exp(-2\alpha_a d_{a\text{-limit}}) \quad (\text{A12})$$

where  $d_{a\text{-limit}}$  is the upper sensing limit as mentioned in Section 4.4. Thus, from Eqs. (A10) and (A12), we can obtain a function between  $D$  and  $d_a$  as

$$D = \left(1 - \frac{\alpha_a}{\alpha_c}\right) d_a + \frac{\alpha_a}{\alpha_c} d_{a\text{-limit}} \quad (\text{A13})$$

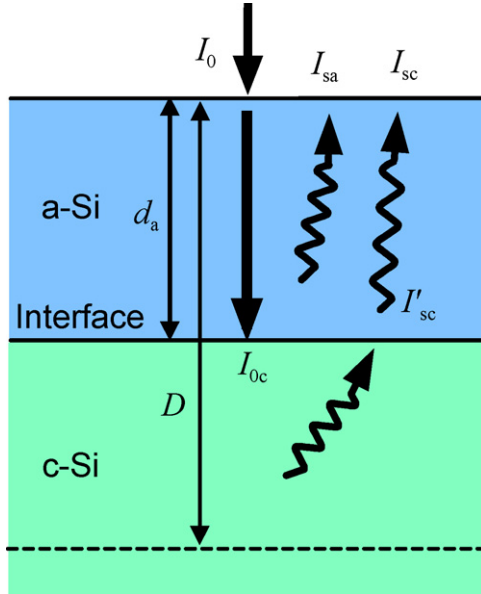


Fig. A4. Double-layer material model for calculating the Raman intensity ratio.

Using Eq. (A13), we can find the maximum sensing depth  $D$  when a near-surface amorphous layer of thickness  $d_a$  exists. In this function,  $d_{a\text{-limit}} \approx 150$  nm according to the experimental results in Section 4.4; the attenuation coefficients for the 532 nm green laser in a-Si and c-Si are  $\alpha_a = 1.5 \times 10^5 \text{ cm}^{-1}$  and  $\alpha_c = 1 \times 10^4 \text{ cm}^{-1}$ , respectively [31].

### A.3. Theoretical Raman intensity ratio

Finally, we discuss the theoretical relationship between the Raman intensity ratio and the thickness of the amorphous layer. As shown in Fig. A4, we consider laser scattering from the amorphous region and that from the crystalline region separately. According to Eq. (A7), the totally scattered light intensity from the amorphous layer should be

$$I_{sa} = \frac{\gamma\sigma_{sa}}{2\alpha_a} I_0 \{1 - \exp(-2\alpha_a d_a)\} \quad (\text{A14})$$

Because the intensity of incident laser at the amorphous-crystalline interface is

$$I_{0c} = I_0 \exp(-\alpha_a d_a) \quad (\text{A15})$$

according to Eq. (A7), the intensity of the upward-scattered light from the crystalline region  $I'_{sc}$  at the amorphous-crystalline interface is

$$\begin{aligned} I'_{sc} &= \frac{\gamma\sigma_{sc}}{2\alpha_c} I_{0c} [1 - \exp\{-2\alpha_c(D - d_a)\}] \\ &= \frac{\gamma\sigma_{sc}}{2\alpha_c} I_0 \exp(-\alpha_a d_a) [1 - \exp\{-2\alpha_c(D - d_a)\}] \end{aligned} \quad (\text{A16})$$

Then the light intensity at the amorphous surface  $I_{sc}$  becomes

$$\begin{aligned} I_{sc} &= I'_{sc} \exp(-\alpha_a d_a) \\ &= \frac{\gamma\sigma_{sc}}{2\alpha_c} I_0 \exp(-2\alpha_a d_a) [1 - \exp\{-2\alpha_c(D - d_a)\}] \end{aligned} \quad (\text{A17})$$

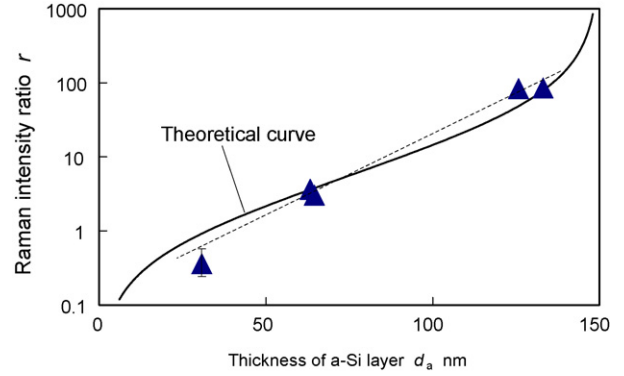


Fig. A5. Comparison between the theoretical relationship and the experimental results of Raman intensity ratio and amorphous layer thickness.

From Eqs. (A9) and (A12), we can obtain the Raman intensity ratio  $r$  as

$$r = \frac{I_{sa}}{I_{sc}} = \frac{\sigma_{sa} \alpha_c}{\sigma_{sc} \alpha_a} \frac{\exp(2\alpha_a d_a) - 1}{1 - \exp\{-2\alpha_c(D - d_a)\}} \quad (\text{A18})$$

If we denote  $\eta$  as the ratio of  $\sigma_{sa}$  to  $\sigma_{sc}$ , and use Eq. (A13) to substitute  $D$  in the above equation, then we obtain

$$r = \eta \frac{\alpha_c}{\alpha_a} \frac{\exp(2\alpha_a d_a) - 1}{1 - \exp\{-2\alpha_a(d_{a\text{-limit}} - d_a)\}} \quad (\text{A19})$$

To determine the value of the constant  $\eta$ , we substituted the experimental data of  $r$  and  $d_a$  in Fig. 7 into Eq. (A19) and the average of  $\eta$  was obtained to be 8.84. Finally, the following equation can be obtained to describe the relationship between the Raman intensity ratio and the depth of the amorphous layer.

$$r = 0.589 \times \frac{\exp(0.03d_a) - 1}{1 - \exp\{-0.03 \times (150 - d_a)\}} \quad (\text{A20})$$

In Fig. A5, the curve of Eq. (A20) is plotted together with the experimental data from Fig. 7. It is clear that the theoretical relationship between the Raman intensity ratio and the amorphous layer thickness approaches a linear one within the range from 20 to 140 nm, and beyond this range nonlinearity occurs. Eq. (A20) can be also deformed into the following equation:

$$d_a = 33.3 \times \ln \left\{ \frac{8.84 + 15r}{8.84 + 0.167r} \right\} \quad (\text{A21})$$

Using Eq. (A21), the thickness of the amorphous layer can be readily calculated from the Raman intensity ratio.

## References

- [1] Kaplan SG, Hanssen LM. Silicon as a standard material for infrared reflectance and transmittance from 2 to 5  $\mu\text{m}$ , *Infra. Phys Technol* 2002;43:389–96.
- [2] Yan J, Syoji K, Kuriyagawa T. Fabrication of large-diameter single-crystal silicon aspheric lens by straight-line enveloping diamond-turning method. *J Jpn Soc Prec Eng* 2002;68(4):1561–5.
- [3] Nakasuji T, Kodera S, Hara S, Matsunaga H, Ikawa N, Shimada S. Diamond turning of brittle materials for optical components. *Ann CIRP* 1990;39(1):89–92.
- [4] Blake PN, Scattergood RO. Ductile regime machining of germanium and silicon. *J Am Ceram Soc* 1990;73(4):949–57.

- [5] Shibata T, Fujii S, Makino E, Ikeda M. Ductile-regime turning mechanism of single-crystal silicon. *Prec Eng* 1996;18(2/3):130–7.
- [6] Yan J, Syoji K, Kuriyagawa T. Chip morphology of ultraprecision diamond turning of single crystal silicon. *J Jap Soc Prec Eng* 1999;65(7):1008–12.
- [7] Yan J, Yoshino M, Kuriyagawa T, Shirakashi T, Syoji K, Komanduri R. On the ductile machining of silicon for micro electro-mechanical systems (MEMS), opto-electronic and optical applications. *Mater Sci Eng A* 2001;297(1/2):230–4.
- [8] Yan J, Syoji K, Kuriyagawa T, Suzuki H. Ductile regime turning at large tool feed. *J Mater Proc Tech* 2002;121:363–72.
- [9] Yan J, Takahashi H, Tamaki J, Gai X, Harada H, Patten J. Nanoindentation tests on diamond-machined silicon wafers. *Appl Phys Lett* 2005;86:181913.
- [10] Yan J, Asami T, Kuriyagawa T. Response of machining-damaged single crystalline silicon wafers to nanosecond pulsed laser irradiation. *Semicond Sci Technol* 2007;22:392–5.
- [11] Ohta T, Yan J, Kuriyagawa T, Kodera S, Nakasuji T. Prediction of subsurface damage depth of ground brittle materials by surface profiling. *Int J Mach Mach Mater* 2007;2(1):108–24.
- [12] Shibata T, Ono A, Kurihara K, Makino E, Ikeda M. Cross-section transmission electron microscope observations of diamond-turned single-crystal Si surfaces. *Appl Phys Lett* 1994;65(20):2553–5.
- [13] Jeynes C, Puttick KE, Whitmore LC, Gartner K, Gee AE, Millen DK, et al. Laterally resolved crystalline damage in single-point-diamond-turned silicon. *Nucl Instrum Meth Phys Res B* 1996;118:431–6.
- [14] Puttick KE, Whitmore LC, Chao CL, Gee AE. Transmission electron microscopy of nanomachined silicon crystals. *Philos Mag A* 1994;69(1):91–103.
- [15] Harris DC, Bertolucci MD. *Symmetry and spectroscopy—an introduction to vibrational and electronic spectroscopy*. Dover Publications; 1989.
- [16] Richter H, Wang ZP, Ley L. The one phonon Raman spectrum in microcrystalline silicon. *Solid State Commun* 1981;39(5):625–9.
- [17] Zwick A, Carles R. Multiple-order Raman scattering in crystalline and amorphous silicon. *Phys Rev B* 1993;48(9):6024–32.
- [18] Needs RJ, Mujica A. First-principles pseudopotential study of the structural phases of silicon. *Phys Rev B* 1995;51(15):9652–60.
- [19] Sparks RG, Paesler MA. Micro-Raman analysis of stress in machined silicon and germanium. *Prec Eng* 1988;10(4):191–8.
- [20] Bismayer U, Brinksmeier E, Güttler B, Seibt H, Menz C. Measurement of subsurface damage in silicon wafers. *Prec Eng* 1994;16(2):139–44.
- [21] Gogotsi Y, Baek C, Kirscht F. Raman microspectroscopy study of processing-induced phase transformations and residual stress in silicon. *Semicond Sci Technol* 1999;14:936–44.
- [22] Gogotsi Y, Zhou G, Ku S, Cetinkunt S. Raman microspectroscopy analysis of pressure-induced metallization in scratching of silicon. *Semicond Sci Technol* 2001;16:345–52.
- [23] Pizani PS, Jasinevicius R, Duduch JG, Porto: AJV. Ductile and brittle modes in single-point-diamond-turning of silicon probed by Raman scattering. *J Mater Sci Lett* 1999;18:1185–7.
- [24] Yan J. Laser micro-Raman spectroscopy of single-point diamond machined silicon substrates. *J Appl Phys* 2004;95(4):2094–101.
- [25] Chen L, Zhang X, Zhang T, Lin H, Lee S. Micro-Raman spectral analysis of the subsurface damage layer in machined silicon wafers. *J Mater Res* 2000;15(7):1441–4.
- [26] Zarudi I, Zhang LC. Effect of ultraprecision grinding on the microstructural change in silicon monocrystals. *J Mater Process Technol* 1998;84:149–58.
- [27] Yan J, Takahashi H, Tamaki J, Gai X, Kuriyagawa T. Transmission electron microscopic observation of nanoindentations made on ductile-machined silicon wafers. *Appl Phys Lett* 2005;87:211901.
- [28] Iqbal Z, Veprek S. Raman scattering from hydrogenated microcrystalline and amorphous silicon. *J Phys C: Solid State Phys* 1982;15:377–92.
- [29] Mei P, Boyce JB, Hack M, Lujan RA, Johnson RI, Anderson GB, et al. Laser dehydrogenation/crystallization of plasma-enhanced chemical vapor deposited amorphous silicon for hybrid thin film transistors. *Appl Phys Lett* 1994;64(9):28–30.
- [30] Saleh R, Nickel NH, Maydell KV. Laser crystallization of compensated hydrogenated amorphous silicon thin films. *J Non-Cryst Solids* 2006;352:1003–7.
- [31] Matsuno A, Takii E, Eto T, Kurobe K, Shibahara K. Merits and demerits of light absorbers for ultra-shallow junction formation by green laser annealing. *Nucl Instr Meth Phys Res B* 2005;237:136–41.